

Effect of external magnetic field on the instability of THz plasma waves in nanoscale graphene field-effect transistors

Liping Zhang(张丽萍), Zongyao Sun(孙宗耀), Jiani Li(李佳妮), and Junyan Su(苏俊燕)

Citation: Chin. Phys. B, 2024, 33 (**4**): 048102. DOI: 10.1088/1674-1056/ad1e66
Journal homepage: http://cpb.iphy.ac.cn; http://iopscience.iop.org/cpb

What follows is a list of articles you may be interested in

Intercalation of hafnium oxide between epitaxially-grown monolayer graphene and Ir(111) substrate

Yi Biao(表奕), Hong-Liang Lu(路红亮), Hao Peng(彭浩), Zhi-Peng Song(宋志朋), Hui Guo(郭辉), and Xiao Lin(林晓)

Chin. Phys. B, 2023, 32 (**9**): 098102. DOI: 10.1088/1674-1056/accff4

Morphological features and nanostructures generated during SiC graphitization process

Wen-Xia Kong(孔雯霞), Yong Duan(端勇), Jin-Zhe Zhang(章晋哲),Jian-Xin Wang(王剑心), and Qun Cai(蔡群)

Chin. Phys. B, 2023, 32 (**6**): 068103. DOI: 10.1088/1674-1056/acb766

Thermoelectric characteristics of flexible reduced graphene oxide/silver selenide nanowire composites prepared by a facile vacuum filtration process

Zuo Xiao(肖佐), Yong Du(杜永), Qiufeng Meng(孟秋风), and Lei Wang(王磊)

Chin. Phys. B, 2022, 31 (**2**): 028103. DOI: 10.1088/1674-1056/ac447e

Magnetoelectric effect in multiferroic $NdMn_2O_5$

Syed Hamad Bukhari, Javed Ahmad

Chin. Phys. B, 2017, 26 (**1**): 018103. DOI: 10.1088/1674-1056/26/1/018103

The effects of static magnetic field on microwave absorption of hydrogen plasma in carbon nanotubes: A numerical study

Peng Zhi-Hua(彭志华), Gong Xue-Yu(龚学余), Peng Yan-Feng(彭延峰), Guo Yan-Chun(郭燕春), and Ning Yan-Tao(宁艳桃)

Chin. Phys. B, 2012, 21 (**7**): 078102. DOI: 10.1088/1674-1056/21/7/078102

Effect of external magnetic field on the instability of THz plasma waves in nanoscale graphene field-effect transistors

Liping Zhang(张丽萍)†, Zongyao Sun(孙宗耀), Jiani Li(李佳妮), and Junyan Su(苏俊燕)

School of Sciences, Lanzhou University of Technology, Lanzhou 730050, *China*

(Received 24 October 2023; revised manuscript received 28 December 2023; accepted manuscript online 15 January 2024)

The instability of plasma waves in the channel of field-effect transistors will cause the electromagnetic waves with THz frequency. Based on a self-consistent quantum hydrodynamic model, the instability of THz plasmas waves in the channel of graphene field-effect transistors has been investigated with external magnetic field and quantum effects. We analyzed the influence of weak magnetic fields, quantum effects, device size, and temperature on the instability of plasma waves under asymmetric boundary conditions numerically. The results show that the magnetic fields, quantum effects, and the thickness of the dielectric layer between the gate and the channel can increase the radiation frequency. Additionally, we observed that increase in temperature leads to a decrease in both oscillation frequency and instability increment. The numerical results and accompanying images obtained from our simulations provide support for the above conclusions.

Keywords: graphene field-effect transistors, external magnetic field, radiation frequency, instability increment

PACS: 81.05.ue, 52.20.–j, 52.35.–g **DOI:** 10.1088/1674-1056/ad1e66

1. Introduction

Over the past few years, THz technologies have been widely developed due to all kinds of potential applications in imaging, biomedicine, communications, security scanning, and so on.[1–5] The THz emission and the THz detection are two important tasks in THz science. In present, there are several types of THz radiation sources, such as, free electron laser that has the advantages of wide spectrum range, high peak power and average power, and good coherence, but is huge in size and inconvenient to use, electro-optic crystal THz pulse source that the THz electromagnetic pulse is radiated on the crystal surface through the optical rectification effect of nonlinear optics, and THz radiation source based on electronic oscillations. In 1993,[6] Dyakonov and Shur reported that the current flow in the channel of ballistic field-effect transistors (FET) will become unstable because of the reflection from the source and the drain, which instability in the gated two-dimensional (2D) electron gas can motivate electromagnetic radiation with THz frequency. So, short-channel FET generating resonant or attenuated plasma waves may act as a kind of efficient THz sources. THz plasma oscillations used for generating and detecting THz radiation in short-channel FET are discussed theoretically and experimentally in Refs. [7,8]. The instability of electron fluid in an FET structure with a gate length of 0.2 μm was investigated using a 2D hydrodynamic model and the results show that the stable periodic oscillations with THz frequencies in the channel were produced.[9]

THz sources that are compact, powerful, tunable, and operating at room temperature are in great demand for many industrial applications and fundamental science, including studying excitations in solids and a plethora of non-equilibrium phenomena.[10,11] Considering this, research on FETs based on common 2D materials, such as graphene, black phosphorus, and molybdenum disulfide, has become widely prevalent.[12,13] For several years great effort has been devoted to the study of the fluid dynamics of electron transport in graphene, which encompass high mobility, shear and hall viscosity, linear response transport, among other things.[14–17] The high electron mobility and massless relativistic dispersion of quasi-particles are widely recognized as the most useful properties of graphene for nanoelectronics applications, suspended graphene and van der Waals heterostructures.[18–24] Additionally, the optical modulation of THz waves was explored in graphene field-effect transistors (GFETs) and GFET THz detectors with room temperature, low impedance, and high sensitivity.[25] All these studies provide compelling evidence that GFETs are excellent devices for both generating and detecting THz radiation. In a recent paper by Justin Crabb,[26] the instable properties of THz plasmas in graphene transistors and the conditions required for DS instability to occur have been analyzed and the results have shown that the coherent anharmonic oscillatory state of the electron fluid has been motivated by instability. In Ref. [27] it was shown that coherent THz frequency combs can be generated and controlled in GFET with asymmetric boundary conditions by using plasma instability that can be controlled by direct current injection. Along with research going deep, it becomes evident that the motion of carrier in the channel of the FET are subjected to the Lorentz force when an external magnetic field is present. It has been reported in literature[28] that the magnetic field will affect the THz emission of nanometer In-

†Corresponding author. E-mail: zhanglp@lut.edu.cn

© 2024 Chinese Physical Society and IOP Publishing Ltd

GaAs/AlInAs high electron mobility transistors. In addition, the effect of magnetic fields on THz emission in GFET and the Hall current caused by magnetic fields are also discussed in Ref. [29], but the effect of magnetic field on nanoscale devices has not been resolved, that is, the quantum effect is neglected. To our knowledge, when the feature size enters the nanometer domain, especially when the feature size of the system is equal to or less than the de Broglie wavelength, the wave functions of the electron overlap. The accompanying tunneling effect, quantum effect, and interference effect are becoming more and more important in devices. The presence of quantum effects will inevitably alter the performance of the device in several ways. A strong quantum mechanical effect due to the channel thickness limitation is experimentally demonstrated in a monolayer MoS_2 FET, supported by the self-consistent calculation.[30] In addition, the effects of quantum effects on instability increment and radiation frequency of THz oscillation were simulated in one-dimensional GFET.[31]

Regarding this paper, we have analyzed and numerically simulated the effects of external magnetic fields and quantum effect on the current instability in the channel of GFET with asymmetric boundary conditions.[32,33] The rest of this article is organized as follows: In Section 2, we innovatively derived a 2D quantum hydrodynamic model (QHM) describing the collective behavior of 2D electron gas in the channel of GFET with the influence of weak magnetic fields. In Section 3, we linearized the quantum hydrodynamic model to obtain the dispersion relation and nondimensional asymmetric boundary conditions. In Section 4, the plasma oscillation instability has been numerically conducted in the channel of GFET under asymmetric boundary conditions with the effects of magnetic fields and quantum effects. It is noteworthy that we also studied the influence of temperature on the instability increment and radiation frequency of THz waves generated in GFET.

2. Model

We employ self-consistent QHM,[34] which originates from Wigner–Poisson systems and has been widely used in the study of quantum plasmas and metallic nanostructures, to describe the collective behavior of 2D graphene electron gas. The continuity equation and the momentum equation are given as follows:

$$\frac{\partial}{\partial t}n+\nabla\cdot(n\boldsymbol{v})=0, \tag{1}$$

$$\frac{\partial}{\partial t}\boldsymbol{v}+\boldsymbol{v}\cdot\nabla\boldsymbol{v}=\frac{\boldsymbol{F}}{m}-\frac{1}{mn}\nabla P+\frac{\hbar^2}{2m^2}\nabla\left(\frac{1}{\sqrt{n}}\nabla^2\sqrt{n}\right), \tag{2}$$

where n is the 2D electronic density, m is the electron effective mass, $\boldsymbol{v}$ is the velocity of electrons, $\boldsymbol{F}$ is the total force exerted on the electron, $\hbar$ is the reduced Planck constant, and P is the pressure stress tensor. The quantum effects are contained in the $\hbar$-dependent term, which refers to the quantum potential (also known as the Bohm potential). It can be derived from the Schrödinger equations. And if we set $\hbar=0$, we can obtain the classical hydrodynamic model. The quantum potential can reveal the wave nature of particles and infer the trajectory of particle motion. As far as we know, magnetic fields do not cause additional quantum effects. According to the previous introduction, quantum effects are related to the size of the system. In addition, according to the literature,[35] the quantum state is regarded as a static flow state and its density is a fixed value in the derivation process.

As mentioned above, the fact that electrons in graphene behave as massless Dirac fermions presents a significant challenge for the development of fluid dynamics models. Specifically, traditional approaches relying on the assumption of mass continuity in fluid dynamics is not applicable to massless particles such as Dirac fermions. Therefore, new theoretical frameworks and mathematical techniques must be developed to address this unique aspect of graphene's electronic properties. Here, the Drude mass[36,37] is used as the effective mass

$$m=\frac{\hbar k_{\mathrm{F}}}{v_{\mathrm{F}}}=\frac{\hbar\sqrt{\pi n}}{v_{\mathrm{F}}}, \tag{3}$$

where $k_{\mathrm{F}}=\sqrt{\pi n}$ is the Fermi momentum in graphene, π is the circumference ratio and v_{F} is the Fermi velocity. This is related to the fact that the band structure of graphene has a linear dispersion relationship, and its effective mass ($m=\hbar k_{\mathrm{F}}/v_{\mathrm{F}}$) can be written in the form of Fermi momentum divided by Fermi velocity, that is, the Drude mass. And it is crucial for our simplification of the pressure term.

For the electron gas in graphene, the most straightforward approximation of the pressure is the statistical pressure encoded in the kinetic energy of the electron gas, and the calculation of pressure (force per unit length in two-dimensions) requires the evaluation of the kinetic energy of the non-interacting gas as[38]

$$K_{\mathrm{g}}=4A\int\frac{\mathrm{d}\theta k\mathrm{d}k}{(2\pi)^2}v_{\mathrm{F}}\hbar k=v_{\mathrm{F}}\hbar\frac{2}{3\pi}\pi^{3/2}N_{\mathrm{e}}^{3/2}A^{-1/2}, \tag{4}$$

where N_{e} is the total number of electrons and A denotes the area of the x–y plane in the system. Hence, the pressure is given by

$$P=-\frac{\partial K_{\mathrm{g}}}{\partial A}=v_{\mathrm{F}}\hbar\frac{1}{3\pi}(\pi n)^{3/2}. \tag{5}$$

Furthermore, the pressure term in Eq. (2) is simplified as

$$-\frac{1}{mn}\nabla P=-\frac{v_{\mathrm{F}}}{\hbar\sqrt{\pi n}}\frac{1}{n}\nabla\left[v_{\mathrm{F}}\hbar\frac{1}{3\pi}(\pi n)^{3/2}\right]=-\frac{v_{\mathrm{F}}^2}{2n}\nabla n. \tag{6}$$

The force term results from the combined effect of the gate and the cyclotron (Lorentz) force

$$\boldsymbol{F}=-e\nabla U_{\mathrm{gate}}+e(\boldsymbol{v}\times\boldsymbol{B}), \tag{7}$$

where e is the elementary charge, $\boldsymbol{B}$ is the magnetic field perpendicular to the 2D graphene electron gas plane and U_{gate} is the gate voltage as given below:[39]

$$U_{\text{gate}} = en\left(\frac{1}{C_{\text{g}}} + \frac{1}{C_{\text{q}}}\right). \tag{8}$$

Here, C_{g} and C_{q} represent the parallel plate capacitance, given by $C_{\text{g}} = \varepsilon/d_0$ and the quantum capacitance, given by $C_{\text{q}} = 2e^2\sqrt{\pi n}/(\pi\hbar v_{\text{F}})$, where $\varepsilon = \varepsilon_0\varepsilon_{\text{graphene}}$ is the dielectric constant of the medium and d_0 is the thickness of the dielectric layer between the gate and the channel. Since the carrier density in graphene is much greater than 10^{12} cm^{-2}, at this point it is quantum capacitors that dominate, $C_{\text{q}} \gg C_{\text{g}}$, and $U_{\text{gate}} = en(d_0/\varepsilon)$.

Consequently, the force term in Eq. (2) is expressed as

$$\frac{\boldsymbol{F}}{m} = -\frac{e^2 d_0}{m\varepsilon}\nabla n + \frac{e}{m}(\boldsymbol{v}\times\boldsymbol{B}). \tag{9}$$

In summary, we get

$$\frac{\partial}{\partial t}n + \nabla\cdot(n\boldsymbol{v}) = 0, \tag{10}$$

$$\frac{\partial}{\partial t}\boldsymbol{v} + \boldsymbol{v}\nabla\boldsymbol{v} = -\frac{e^2 d_0}{m\varepsilon}\nabla n + \frac{e}{m}(\boldsymbol{v}\times\boldsymbol{B}) - \frac{v_{\text{F}}^2}{2n}\nabla n + \frac{\hbar}{2m^2}\nabla\left(\frac{1}{\sqrt{n}}\nabla^2\sqrt{n}\right). \tag{11}$$

3. Dispersion relation

Owing to the small amplitude of the oscillations, and terms containing higher powers of amplitude factors can be neglected, we separate the dependent variables into two parts: an "equilibrium" part indicated by a subscript 0, and a "perturbation" part indicated by a subscript 1. This allows us to investigate the oscillations of THz plasmon waves in the channel of a quantum GFET:[40] $n = n_0 + n_1$, $v_x = v_{x0} + v_{x1}$, $v_y = v_{y1}$ with n_1, v_{x1}, $v_{y1} \sim \exp(-\mathrm{i}\omega t + \mathrm{i}kx + \mathrm{i}qy)$, where ω is the frequency, k and q are the components of the wave vector in the x and y directions, The linearized equation is shown below:

$$(\omega - kv_{x0})n_1 - kn_0 v_{x1} - qn_0 v_{y1} = 0, \tag{12}$$

$$(\omega - kv_{x0})v_{x1} - \mathrm{i}\omega_{\text{c}}v_{y1} = s^2\frac{n_1}{n_0}k + \frac{\hbar^2 n_1}{4m^2 n_0}k(k^2+q^2), \tag{13}$$

$$(\omega - kv_{x0})v_{y1} + \mathrm{i}\omega_{\text{c}}v_{x1} = s^2\frac{n_1}{n_0}q + \frac{\hbar^2 n_1}{4m^2 n_0}q(k^2+q^2), \tag{14}$$

where $\omega_{\text{c}} = (e/m)B$ is the cyclotron frequency and

$$s^2 = \frac{e^2 d_0 n_0}{m\varepsilon} + \frac{v_{\text{F}}^2}{2}$$

can be interpreted as the sound velocity of the carrier's fluid. Then, for the convenience of computation, we nondimensionalize the above Eqs. (12)–(14). The dimensionless physical quantities are: $x \sim L$, $s \sim v_0$, $t \sim L/v_0$, $n \sim n_0$, $v \sim v_0$, $\omega \sim v_0/L$, k, $q \sim 1/L$, where L is the channel length. This procedure gives

$$(\Omega - \tilde{k})\tilde{n}_1 - \tilde{k}\tilde{v}_{x1} - \tilde{q}\tilde{v}_{y1} = 0, \tag{15}$$

$$(\Omega - \tilde{k})\tilde{v}_{x1} - \mathrm{i}\Omega_{\text{c}}\tilde{v}_{y1} = \left[H\tilde{k}(\tilde{k}^2+\tilde{q}^2) + \beta^2\tilde{k}\right]\tilde{n}_1, \tag{16}$$

$$(\Omega - \tilde{k})\tilde{v}_{y1} + \mathrm{i}\Omega_{\text{c}}\tilde{v}_{x1} = \left[H\tilde{q}(\tilde{k}^2+\tilde{q}^2) + \beta^2\tilde{q}\right]\tilde{n}_1. \tag{17}$$

Further derivation leads to the non-dimensional dispersion equation

$$-(\Omega - \tilde{k})^2 + \Omega_{\text{c}}^2 + H\left(\tilde{k}^2+\tilde{q}^2\right)^2 + \beta^2(\tilde{k}^2+\tilde{q}^2) = 0, \tag{18}$$

where $\Omega = \omega L/v_0$, $\tilde{k}$ and $\tilde{q}$ are non-dimensional frequency and wave vectors in x and y directions, respectively. $\Omega_{\text{c}} = \omega_{\text{c}}L/v_0$ is the dimensionless cyclotron frequency, $\beta = s/v_0$ is the velocity of sound after dimension lessness, and for simplicity, the following β are collectively referred to as Mach numbers (since s is greater than v_0, β starts with 1). $H = \hbar^2/4m^2v_0^2L^2$ corresponds to quantum effects controlled by the channel length. It can be seen from Eq. (18) that $\tilde{k}$ has four roots. However, numerical results indicate that $\tilde{k}$ has only two feasible roots, $\tilde{k}_1$ and $\tilde{k}_2$.

Research in Ref. [6] indicated that the currents in the channel of FET will instable under asymmetric boundary conditions, which leads to the generation of THz waves. The asymmetric boundary condition arises from the highly asymmetrical impedance of the source and drain of the cavity, that is, the source approaches 0 and the drain approaches infinity.[32] Then, the boundary conditions are

$$n_1(0) = 0, \quad n_0 v_1(L) + v_0 n_1(L) = 0. \tag{19}$$

This boundary condition corresponds to a short circuit at the source electrode and an open circuit at the drain electrode, and it can be realized by grounding the source either directly or via very large capacitance presenting a short at plasma wave frequencies and by attaching the drain to the power supply via an inductance that presents an open circuit at plasma wave frequencies. From Eq. (19), we obtain

$$\exp[\mathrm{i}(\tilde{k}_2 - \tilde{k}_1)] = \frac{\tilde{k}_2}{\tilde{k}_1}. \tag{20}$$

Using the above equation, we can determine the real and imaginary parts of the complex frequency $\Omega = \Omega' + \mathrm{i}\Omega''$, whose sign of the imaginary part Ω'' will determine the stability of the steady state. A positive imaginary part $\Omega'' > 0$ corresponds to instability.[41] Typically, both the instability increment and the radiation frequency depend on the magnetic field, wave vector in the y direction, quantum effects, the thickness of the dielectric layer between the gate and the channel length and the temperatures.

4. Numerical result

To analyze the fundamental characteristics of plasma waves in the channel of GFET, we numerically solve Eqs. (18) and (20).

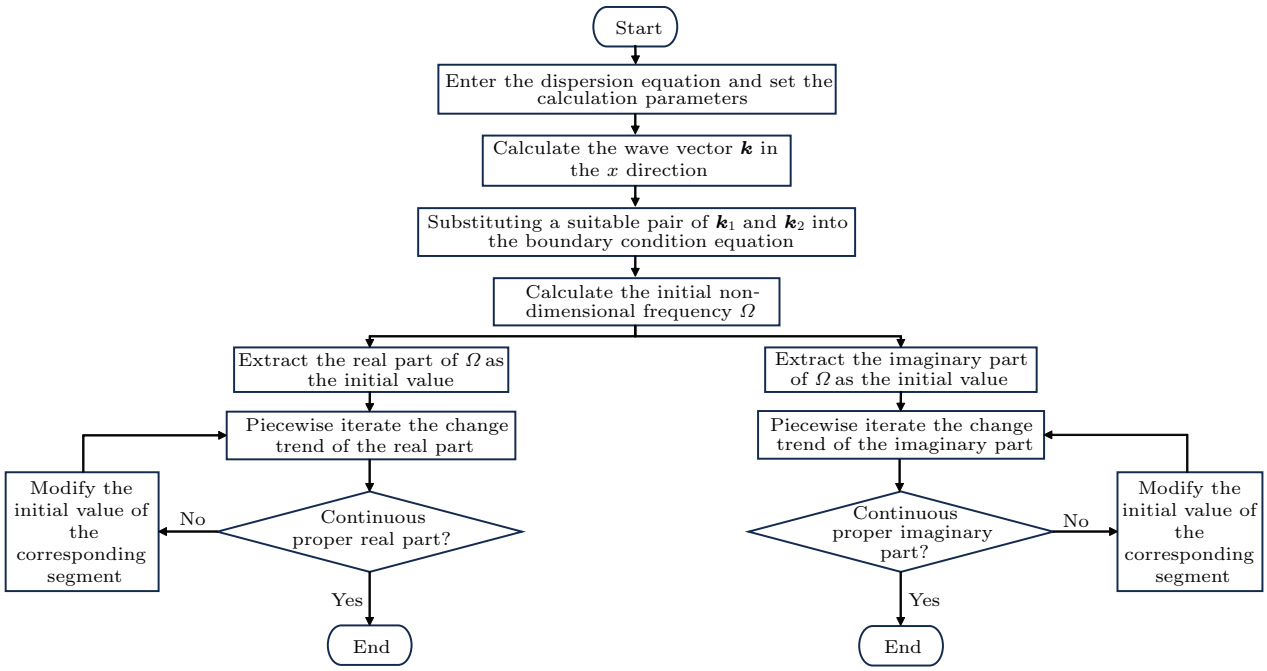


Fig. 1. Simulation structure diagram.

Table 1. The device parameters.

Parameters	Values
L (the channel length)	1×10^{-7} m
d_0 (the thickness of the dielectric layer between the gate and the channel)	2×10^{-8} m
W (the width of channel)	5×10^{-6} m
$\varepsilon_{\text{graphene}}$ (graphene's permittivity)	4.5
v_{F} (the Fermi velocity)	1×10^{6} m/s
n_0 (the carrier concentration of graphene)	3×10^{16} m^{-2}
m (the effective mass of graphene)	3.22×10^{-32} kg
B (the magnetic induction intensity)	1 T

The numerical results are shown in Figs. 2–8. The dotted lines in the figures correspond to the instability increment on left, and the broken lines correspond to the radiation frequency on right. Figures 2–5 illustrate the dependencies of the instability increment and radiation frequency on the Mach number β for different external magnetic field $\boldsymbol{B}$, wave vector in the y direction q, and the quantum effect H. It is obvious that the instability increment and radiation frequency of THz plasma oscillation increases with β. From Figs. 2 and 3, we can see that the magnetic field $\boldsymbol{B}$ reduces the instability increment but enhances the radiation frequency. The lower instability increment corresponds to the lower emission intensity. So the presence of magnetic fields suppressed the emission intensity, which is similar with the experiment result.[28] Furthermore, it can be seen from Fig. 2 that the effect of magnetic field $\boldsymbol{B}$ on the instability increment and radiation frequency is relatively significant in the transonic regime, but that is less noticeable in the subsonic case. It has been mentioned in the literature[28] that the geometric magnetoresistance $\Delta R_t(B)$ generated when a magnetic field is applied to an FET. The expression of geometric magnetoresistance is $\Delta R_t(B) = L_{\text{sd}}\mu_0 B^2/(en_0W)$. According to calculation parameter ($L_{\text{sd}} = L = 10^{-7}$ m, $\mu_0 = 1.5$ m^2/V·s, $B = 1$ T, $e = 1.6\times10^{-19}$ C, $n_0 = 3\times10^{16}$ m^{-2}, $W = 5\times10^{-6}$ m), where μ_0 is the electron mobility of graphene and W is the width of channel, we can get: $\Delta R_t(B) = L_{\text{sd}}\mu_0 B^2/(en_0W) = 6.2\ \Omega$, and this is a smaller resistance value compared to the resistance of the FET, which makes the effect of $\Delta R_t(B) = 6.2\ \Omega$ on THz waves weak.

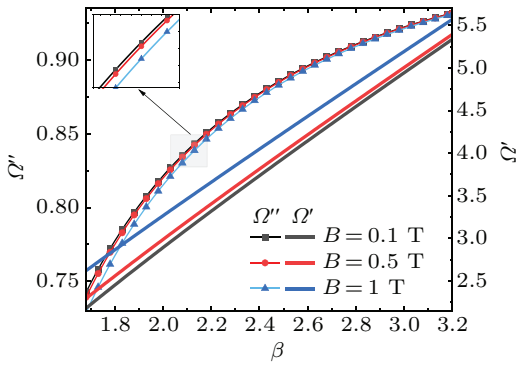


Fig. 2. The instability increment Ω'' and radiation frequency Ω' *versus* β for different $\boldsymbol{B}$ with $q = 0.9$, $H = 0.003$, and the dotted lines in the figure correspond to the instability increment on left, and the broken lines correspond to the radiation frequency on right.

From Fig. 4 it can be observed that the y directional wave vector q reduces the instability increment but enhances the radiation frequency. As shown in Fig. 4, the influence of the y directional wave vector q on instability increment is similar to Fig. 2, but the influence of q on the radiation frequency is opposite. Consider Fig. 5, which plots the instability increment and radiation frequency *versus* β with different quantum effects, H. Figure 5 indicates that the increase of quantum effect

results in an increase in the instability increment and radiation frequency, and the influence of the quantum effects on the characteristics of unstable THz plasma wave is more obvious in the transonic region. With the continuous reduction of device size, quantum effect become more pronounced. That is, the radiation power and frequency of THz wave can be adjusted by changing the size of GFET.

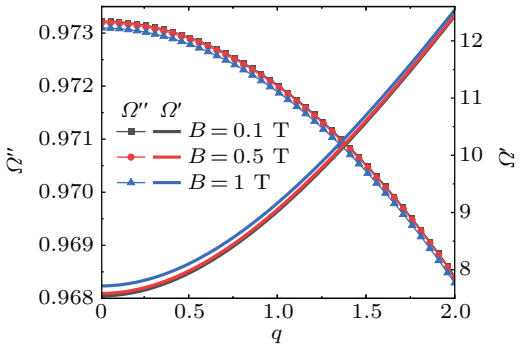


Fig. 3. The instability increment Ω'' and radiation frequency Ω' *versus* q for different $\boldsymbol{B}$ with $\beta = 5$, $H = 0.003$, and the dotted lines in the figure correspond to the instability increment on left, and the broken lines correspond to the radiation frequency on right.

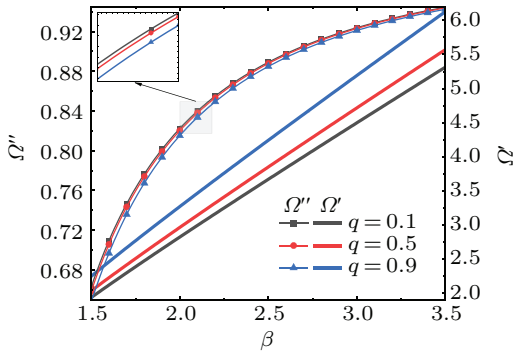


Fig. 4. The instability increment Ω'' and radiation frequency Ω' *versus* β for different q with $\boldsymbol{B} = 1$ T, $H = 0.003$, and the dotted lines in the figure correspond to the instability increment on left, and the broken lines correspond to the radiation frequency on right.

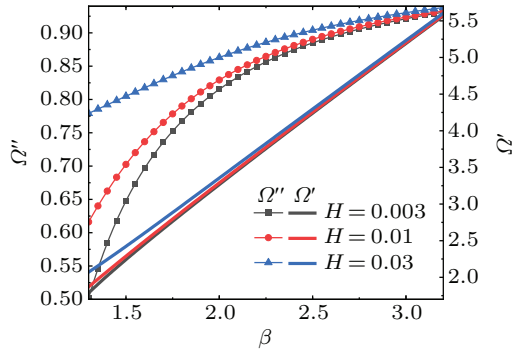


Fig. 5. The instability increment Ω'' and radiation frequency Ω' *versus* β for different H with $q = 0.9$, $\boldsymbol{B} = 1$ T, and the dotted lines in the figure correspond to the instability increment on left, and the broken lines correspond to the radiation frequency on right.

In Fig. 6, we show the dependencies of the instability increment and radiation frequency on the dimensionless cyclotron frequency Ω_c at different quantum effects H. It can be seen from Fig. 6 that the instability increment slightly decreases with the increase of the strength of magnetic field, while the radiation frequency increases. Figure 6 indicates that when the strength of magnetic field is relatively strong, the variation of the radiation frequency with the magnetic field is obvious.

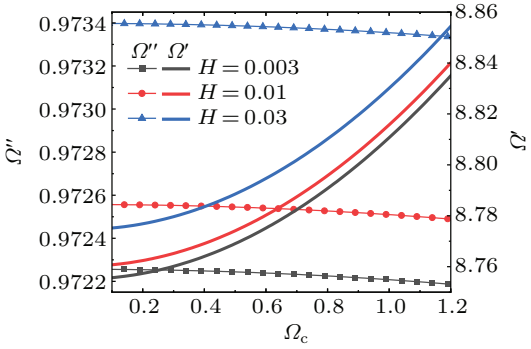


Fig. 6. The instability increment Ω'' and radiation frequency Ω' *versus* Ω_c for different H with $q = 0.9$, $\beta = 5$, and the dotted lines in the figure correspond to the instability increment on left, and the broken lines correspond to the radiation frequency on right.

In Fig. 7, we show the dependencies of the instability increment and radiation frequency on the quantum effects H at different values of the thickness of the dielectric layer between the gate and the channel d_0. It can be seen from Fig. 7 that the instability increment and the radiation frequency increase with the increase of d_0. We can also observe that quantum effects have a more pronounced impact on the instability increment for thinner dielectric layer, and as the quantum effects increases, the influence of the thickness of the dielectric layer on the instability increment will diminish.

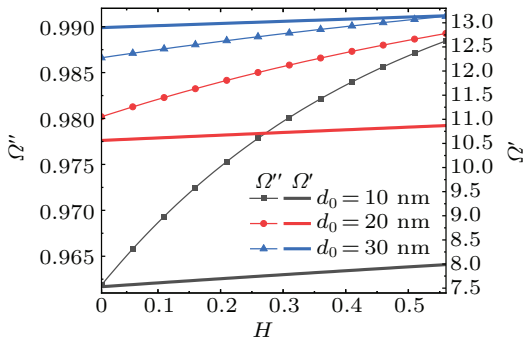


Fig. 7. The instability increment Ω'' and radiation frequency Ω' *versus* H for different d_0 with $q = 0.9$, $\boldsymbol{B} = 1$ T, and the dotted lines in the figure correspond to the instability increment on left, and the broken lines correspond to the radiation frequency on right.

The temperature T has a significant impact on the performance of GFET.[42] We proceed from the indisputable fact that graphene is a metal-like material with zero band gap between the valence band and the conduction band,[43] and further analyzed based on the Fermi–Dirac distribution of the 2D metal electron gas.

The relationship between the concentration of free electrons and the Fermi energy (E_F) can be obtained based on the

Fermi–Dirac distribution function and the density of states in a 2D system

$$n = \int N(E) f(E) \mathrm{d}E = \frac{m}{\pi\hbar^2} E_{\mathrm{F}}.$$

We also found that v_{F} is also determined by E_{F}

$$v_{\mathrm{F}} = \frac{\hbar k_{\mathrm{F}}}{m} = \frac{\sqrt{2mE_{\mathrm{F}}}}{m} = \sqrt{\frac{2E_{\mathrm{F}}}{m}},$$

and E_{F} is controlled by temperature T as

$$E_{\mathrm{F}} = E_{\mathrm{F}}^0 \left[1 - \frac{\pi^2}{12}\left(\frac{k_{\mathrm{B}}T}{E_{\mathrm{F}}^0}\right)^2\right].$$

Here, E_{F}^0 represents the Fermi energy level at 0 K, and k_{B} is the Boltzmann constant.

In Fig. 8, we show the dependencies of the instability increment and radiation frequency on the quantum effects H at different temperatures T. One can see from Fig. 8 that when the temperatures T rise the instability increment and the radiation frequency decrease. According to the literature,[44] an increase in temperature leads to a decrease in electron mobility and the movement of carriers in the channel will be limited. The reduction in mobility weakens the potential of DS instability associated with THz radiation.

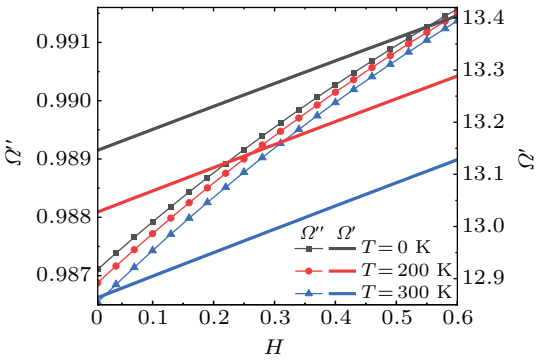


Fig. 8. The instability increment Ω'' and radiation frequency Ω' *versus* H for different T with $q = 0.9$, $\boldsymbol{B} = 1$ T, and the dotted lines in the figure correspond to the instability increment on left, and the broken lines correspond to the radiation frequency on right.

5. Conclusion

In summary, based on a quantum hydrodynamic model, we extensively studied current instability and THz wave generation in GFET with an external magnetic field. A dispersion relation was obtained by a quantum hydrodynamic model describing the collective behavior of 2D electron gas in the channel of GFET. To obtain the dependence of the characteristics of THz plasma wave on physic factors, we gave the solution of transcendental equation under asymmetric boundary condition. The numerical results indicate that the external magnetic field, wave vector along y axis, quantum effects, dielectric layer thickness between gate and channel, as well as temperature have influence on the instability increment and the radiation frequency of the plasma wave in the channel of GFET. The quantum effects and the width of dielectric layer between the gate and the channel cause to the instability increment and the radiation frequency of THz oscillation increase; the increase in temperature cuts the instability increment and the radiation frequency; the magnetic field and wave vector along y axis reduce the instability increment but increase the radiation frequency. It is feasible to regulate the instability increment and the radiation frequency by adjusting the magnetic field. The obtained results allow us to determine device parameters required for the experimental observation of the instability. These properties could make the GFET advantageous for realization of practical THz oscillations.

Acknowledgements

Project supported by the National Natural Science Foundation of China (Grant No. 12065015) and the Hongliu First-level Discipline Construction Project of Lanzhou University of Technology.

References

[1] Hosseininejad S E, Neshat M, Faraji-Dana R, Lemme M, Bolivar P H, Cabellos-Aparicio A, Alarcon E and Abadal S 2018 *Nanomaterials* **8** 577
[2] Liu W Q, Lu Y F, Jiao G H, Chen X F, Zhou Z S, She R B, Li J Y, Chen S H, Dong Y M and Lv J C 2016 *Chin. Phys. B* **25** 060702
[3] Dhillon S S, Vitiello M S, Linfield E H, *et al.* 2017 *J. Phys. D: Appl. Phys.* **50** 043001
[4] Leitenstorfer A, Moskalenko A S, Kampfrath T, *et al.* 2023 *J. Phys. D: Appl. Phys.* **56** 223001
[5] Zhao J W, He M X, Dong L J, Li S X, Liu L Y, Bu S C, Ouyang C M, Wang P F and Sun L L 2019 *Chin. Phys. B* **28** 048703
[6] Dyakonov M and Shur M 1993 *Phys. Rev. Lett.* **71** 2465
[7] Dyakonov M I 2010 *C. R. Phys.* **11** 413
[8] Knap W, Dyakonov M, Coquillat D, Teppe F, Dyakonova N, Łusakowski J, Karpierz K, Sakowicz M, Valusis G, Seliuta D, Kasalynas I, Fatimy A EI, Meziani Y M and Otsuji T 2009 *J. Infrared Millim. Te.* **30** 1319
[9] Dmitriev A P, Furman A S, Kachorovskii V Yu, Samsonidze G G and Samsonidze Ge G 1997 *Phys. Rev. B* **55** 10319
[10] Mendl C B, Polini M and Lucas A 2021 *Appl. Phys. Lett.* **118** 013105
[11] Otsuji T, Popov V and Ryzhii V 2014 *J. Phys. D: Appl. Phys.* **47** 094006
[12] Wang X R, Yi S and Zhang R 2013 *Chin. Phys. B* **22** 098505
[13] Li X F, Xiong X and Wu Y Q 2017 *Chin. Phys. B* **26** 037307
[14] Svintsov D, Vyurkov V, Ryzhii V and Otsuji T 2013 *Phys. Rev. B* **88** 245444
[15] Lucas A and Fong K C 2018 *J. Phys.: Condens. Matter* **30** 053001
[16] Torre I, Tomadin A, Geim A K and Polini M 2015 *Phys. Rev. B* **92** 165433
[17] Levitov L and Falkovich G 2016 *Nat. Phys.* **12** 672
[18] Hosen K, Islam M R and Liu K 2020 *Chin. J. Chem. Phys.* **33** 757
[19] Narozhny B N, Gornyi I V, Mirlin A D and Schmalian J 2017 *Ann. Phys.* **529** 1700043
[20] Vicarelli L, Vitiello M S, Coquillat D, Lombardo A, Ferrari A C, Knap W, Polini M, Pellegrini V and Tredicucci A 2012 *Nat. Mater.* **11** 865
[21] Schwierz F 2010 *Nat. Nanotechnol.* **5** 487
[22] Müller M, Schmalian J and Fritz L 2009 *Phys. Rev. Lett.* **103** 025301
[23] Yamoah M A, Yang W M, Pop E and Goldhaber-Gordon D 2017 *ACS Nano* **11** 9914

[24] Bandurin D A, Torre I, Kumar R K, Shalom M B, Tomadin A, Principi A, Auton G H, Khestanova E, Novoselov K S, Grigorieva I V, Ponomarenko L A, Geim A K and Polini M 2016 *Science* **351** 1055

[25] Viti L, Purdie D G, Lombardo A, Ferrari A C and Vitiello M S 2020 *Nano Lett.* **20** 3169

[26] Crabb J, Cantos-Roman X, Jornet J M and Aizin G R 2021 *Phys. Rev. B* **104** 155440

[27] Cosme P and Tercas H 2020 *ACS Photon.* **7** 1375

[28] Dyakonova N, Teppe F, Łusakowski J, Knap W, Levinshtein M, Dmitriev A P, Shur M S, Bollaert S and Cappy A 2005 *J. Appl. Phys.* **97** 114313

[29] Cosme P and Tercas H 2021 *Appl. Phys. Lett.* **118** 131109

[30] Fang N and Nagashio K 2020 *2D Mater.* **7** 014001

[31] Zhang L P, Feng J X, Liu C X and Su J Y 2022 *Chin. J. Phys.* **75** 104

[32] Zhang L P and Xue J K 2013 *Phys. Plasmas* **20** 082118

[33] Haas F 2005 *Phys. Plasmas* **12** 062117

[34] Manfredi G 2005 *Fields Inst. Commun.* **46** 263

[35] Madelung E 1926 *Z. Phys.* **40** 322

[36] Figueiredo J L, Bizarro J P S and Tercas H 2022 *New J. Phys.* **24** 023026

[37] Castro Neto A H, Guinea F, Peres N M R, Novoselov K S and Geim A K 2009 *Rev. Mod. Phys.* **81** 109

[38] Chaves A J, Peres N M R, Smirnov G and Mortensen N A 2017 *Phys. Rev. B* **96** 195438

[39] Zhu W J, Perebeinos V, Freitag M and Avouris P 2009 *Phys. Rev. B* **80** 235402

[40] Chen F F 2016 *Introduction to plasma physics and controlled fusion* (Switzerland: Springer International Publishing) pp. 51–88

[41] Kushwaha M S and Vasilopoulos P 2001 *Phys. Rev. B* **64** 125320

[42] Novoselov K S, Geim A K, Morozov S V, Jiang D, Katsnelson M I, Grigorieva I V, Dubonos S V and Firsov A A 2005 *Nature* **438** 197

[43] Chen X Y, Tian Z, Li Q, Li S X, Zhang X Q, Ouyang C M, Gu J Q, Han J G and Zhang W L 2020 *Chin. Phys. B* **29** 077803

[44] Zhu W J, Perebeinos V, Freitag M and Avouris P 2009 *Phys. Rev. B* **80** 235402